

Direct Thermal to Electrical Energy Conversion Using 9.5/65/35 PLZT Ceramics in the Ergodic Relaxor Phase

Thomas K. Chin, Felix Y. Lee, Ian M. McKinley, Sam Goljahi, Christopher S. Lynch, and Laurent Pilon

Abstract—This paper reports on direct thermal to electrical energy conversion by performing the Olsen cycle on 9.5/65/35 lead lanthanum zirconate titanate (PLZT). The Olsen cycle consists of two isothermal and two isoelectric field processes in the electric displacement versus electric field diagram. It was performed by alternatively dipping the material in hot and cold dielectric fluid baths under specified electric fields. The effects of applied electric field, sample thickness, electrode material, operating temperature, and cycle frequency on the energy and power densities were investigated. A maximum energy density of 637 ± 20 J/L/cycle was achieved at 0.054 Hz with a 250- μm -thick sample featuring Pt electrodes and coated with a silicone conformal coating. The operating temperatures varied between 3°C and 140°C and the electric field was cycled between 0.2 and 6.0 MV/m. A maximum power density of 55 ± 8 W/L was obtained at 0.125 Hz under the same operating temperatures and electric fields. The dielectric strength of the material, and therefore the energy and power densities generated, increased when the sample thickness decreased from 500 to 250 μm . Furthermore, the electrode material was found to have no significant effect on the energy and power densities for samples subject to the same operating temperatures and electric fields. However, samples with electrode material possessing thermal expansion coefficients similar to that of PLZT were capable of withstanding larger temperature swings. Finally, a fatigue test showed that the power generation gradually degraded when the sample was subject to repeated thermoelectrical loading.

I. INTRODUCTION

LARGE amounts of waste heat are released from power generation, heating, refrigeration, and heat pump cycles as a direct consequence of the second law of thermodynamics. It was estimated that 58% of the energy consumed in the United States in 2009 was lost as waste heat, which was typically discharged to the environment [1]. More than 80% of this waste heat was produced by electricity generation and transportation systems. It could be advantageous to harvest this free source of energy so that the overall energy efficiency of these systems can be increased.

Manuscript received February 15, 2012; accepted July 19, 2012.

F. Y. Lee is indebted to the UCLA Mechanical and Aerospace Engineering Department for financial support in the form of a graduate fellowship. I. M. McKinley was supported in part by the NSF-IGERT program Clean Energy for Green Industry at UCLA.

The authors are with the Mechanical and Aerospace Engineering Department, Henry Samueli School of Engineering and Applied Science, University of California, Los Angeles, CA (e-mail: pilon@seas.ucla.edu).

DOI <http://dx.doi.org/10.1109/TUFFC.2012.2470>

The pyroelectric effect consists of directly converting thermal energy into electrical energy. In practice, the generated energy can be harvested by delivering it to an external load or storage unit. For example, the circuit proposed by Lallart *et al.* [2] to harvest dc power produced by electrostrictive materials on a load could be adapted. A wide range of pyroelectric materials exists which have been used for various applications including infrared sensors [3]–[5], optical memory [4], [6], multi-layer capacitors [7], [8], and energy harvesters [9]–[34]. An important effort in developing pyroelectric energy conversion consists of identifying the pyroelectric materials capable of generating the largest amount of energy and power for a given temperature range.

The present study reports experimental measurements of the pyroelectric energy and power generation capabilities of 9.5/65/35 lead lanthanum zirconate titanate (PLZT). The effects of various operating parameters were systematically investigated.

II. BACKGROUND

A. Pyroelectricity

Pyroelectric materials possess a spontaneous polarization defined as the average dipole moment per unit volume. A subclass of pyroelectric materials, known as ferroelectric materials, have the ability to switch the direction and magnitude of their spontaneous polarization by reversing the applied coercive electric field [35]. A ferroelectric material undergoes a phase transition from ferroelectric to paraelectric when it is heated above its Curie temperature, T_{Curie} . The Curie temperature is typically defined as the temperature corresponding to the maximum complex dielectric constant for a specified frequency and applied electric field [36]. The spontaneous polarization is a temperature-dependent property, becoming negligibly small as the temperature increases beyond T_{Curie} . Fig. 1 shows the unipolar isothermal hysteresis curves between electric displacement and electric field (D - E) for a ferroelectric material at temperatures T_{hot} and T_{cold} . The D - E loops travel in a counter-clockwise direction upon cycling of the electric field within the material while its temperature is held constant. The electric displacement D of an isotropic material at electric field E and temperature T can be expressed as [35], [37]

$$D(E, T) = \epsilon_0 \epsilon_r(E, T)E + P_s(T), \quad (1)$$

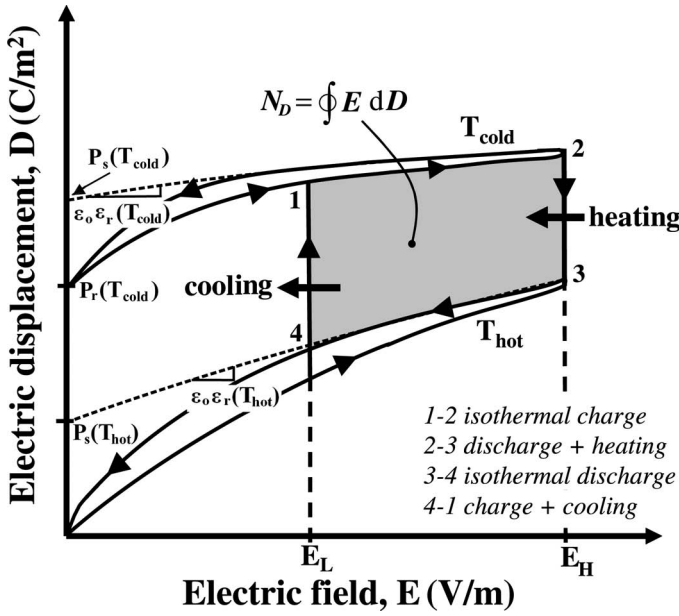


Fig. 1. Isothermal unipolar electric displacement versus electric field (D - E) hysteresis loops for a typical pyroelectric material at temperatures T_{cold} and T_{hot} along with the Olsen cycle. The electrical energy generated per cycle is represented by the area enclosed by 1–2–3–4.

where ε_0 is the vacuum permittivity ($= 8.854 \times 10^{12}$ F/m) and $\varepsilon_r(E, T)$ is the relative permittivity of the material at electric field E and temperature T . The saturation polarization, denoted by $P_s(T)$, is estimated as the displacement in the linear fit of D versus E extrapolated at zero electric field. The slope of this linear fit corresponds to the product $\varepsilon_0 \varepsilon_r(E, T)$, as illustrated in Fig. 1.

B. Olsen Cycle

The Olsen cycle is comprised of four processes as illustrated in Fig. 1. Process 1–2 consists of isothermally charging the pyroelectric element (PE) at T_{cold} by increasing the electric field from E_L to E_H . Then, the sample is discharged in process 2–3 as the element is heated from T_{cold} to T_{hot} under constant electric field E_H . Process 3–4 consists of decreasing the electric field from E_H to E_L under isothermal conditions at T_{hot} . Finally, process 1–4 closes the cycle by cooling the sample from T_{hot} to T_{cold} under constant electric field E_L . This clockwise loop encloses the area bounded by the isothermal D - E curves at T_{hot} and T_{cold} . Its area represents the energy generated per unit volume of material per cycle (in J/L/cycle) expressed as [12]

$$N_D = \oint E dD. \quad (2)$$

The power density P_D (in W/L) produced is then defined as

$$P_D = N_D f, \quad (3)$$

where f is the cycle frequency. It is evident that 1) increasing T_{hot} and decreasing T_{cold} and/or 2) increasing

the electric field span ($E_H - E_L$) results in larger energy generated. However, this is limited by the thermoelectromechanical stress that the sample can withstand.

Olsen and coworkers designed and built several prototypical pyroelectric energy converters implementing the Olsen cycle [10],[12]–[14], [38]. For example, Olsen *et al.* [9], [10], [12]–[14] assembled a regenerative and multistage device using 250- μm -thick lead zirconate stannate titanate (PZST). The electric field was cycled between 0.4 and 2.8 MV/m. The temperatures of the cold and hot sources were 145°C and 178°C, respectively. A piston was used to vertically oscillate a working fluid between a hot and a cold source [10]. This device achieved a maximum power density of 33.9 W/L at 0.26 Hz. Moreover, because of the high cost of PZST per watt generated, Olsen *et al.* [38] built a device using inexpensive 73/27 mol.% P(VDF-TrFE) films. The maximum power density output of this device was 2.38 W/L at 0.079 Hz, while operating at temperatures between 20°C and 90°C and electric fields between 23 and 53 MV/m. More recently, Nguyen *et al.* [28] assembled and operated a prototypical device using commercial 60/40 P(VDF-TrFE) as the pyroelectric material and 50-cSt silicone oil as the working fluid. The maximum power density obtained was 10.7 W/L at 0.12 Hz between 67.3°C and 81.4°C and 20.2 and 37.9 MV/m.

C. Dipping Experiments

Successive dipping of a PE into hot and cold dielectric fluid baths under specified electric fields provides a simple and somewhat idealized way to perform the Olsen cycle. It can be used to assess the energy and power generation performance of pyroelectric materials before using them in actual devices. Table I summarizes the power density obtained using the Olsen cycle for different materials, temperature ranges, operating electric fields, and frequencies as reported in the literature.

Olsen *et al.* [9] performed such dipping experiments on 70- to 100- μm -thick 60/40 P(VDF-TrFE) films in hot and cold 100-cSt silicone oil baths at 25°C and 100°C to 120°C, respectively. The low electric field was kept constant at 0.2 MV/m and the high electric field E_H varied between 20 and 60 MV/m. A maximum output energy density of 900 J/L/cycle was reported at 0.125 Hz for $T_{\text{hot}} = 120^\circ\text{C}$ and $E_H = 50$ MV/m. This corresponds to a power density of 112.5 W/L. However, it remains unclear whether these experimental results were averaged over multiple cycles and if they were repeatable.

More recently, Ikura [17] reported a maximum power density of 13.3 W/L for 60/40 P(VDF-TrFE) subjected to dipping experiments at 0.256 Hz. The operating temperatures were between 58°C and 76°C while the electric field was cycled between 4 and 48 MV/m. Khodayari *et al.* [22] performed the Olsen (or Ericsson) cycle on [110]-poled single crystal PZN-4.5PT and generated 24.4 W/L at 0.1 Hz for temperatures between 100°C and 160°C and electric field between 0 and 1.0 MV/m. Meanwhile, Navid and Pilon [26] performed the Olsen cycle on commercial, puri-

TABLE I. SUMMARY OF MAXIMUM POWER DENSITY OBTAINED USING THE OLSEN CYCLE FOR DIFFERENT MATERIALS, TEMPERATURE RANGES, OPERATING ELECTRIC FIELDS, AND FREQUENCIES.

Material	T_{cold} (°C)	T_{hot} (°C)	E_L (MV/m)	E_H (MV/m)	f (Hz)	P_D (W/L)	Ref.
PZST	156.8	177.4	0.4	2.8	0.26	33.9	[48]
73/27 P(VDF-TrFE)	23.0	67.0	23.0	53.0	0.079	2.38	[49]
60/40 P(VDF-TrFE)	25.0	120.0	20.0	50.0	0.125	112.5	[47]
60/40 P(VDF-TrFE)	58.3	76.5	4.0	48.0	0.256	13.3	[22]
60/40 P(VDF-TrFE)	67.3	81.4	20.2	37.9	0.12	10.7	[43]
60/40 P(VDF-TrFE)	25.0	120.0	20.0	50.0	0.13	58.0	[41]
PZN-4.5PT	100.0	160.0	0.0	1.0	0.10	24.3	[25]
PZN-5.5PT	100.0	190.0	0.0	1.5	0.10	11.7	[38]
PMN-32PT	80.0	170.0	0.2	0.9	0.049	4.92	[24]
8/65/35 PLZT	25.0	160.0	0.2	7.5	0.0178	15.8	[32]
9.5/65/35 PLZT	3.0	140.0	0.2	6.0	0.125	55.3	Present study

fied, and porous 60/40 P(VDF-TrFE) films under quasi-equilibrium conditions. Quasiequilibrium refers to operations in which the electric displacement reached a steady state during isoelectric field heating (process 2–3) and cooling (process 4–1) before the electric field was varied to perform processes 3–4 and 1–2, respectively. The 60/40 P(VDF-TrFE) films were dipped into cold and hot 50-cSt silicone oil baths at 25°C and 100°C to 120°C, respectively. The low electric field was $E_L = 20$ MV/m and the high electric field E_H varied between 30 and 60 MV/m. The maximum power density generated were 58, 36, and 18 W/L for commercial, purified, and porous films, respectively [26]. In addition, Kandilian *et al.* [24] studied the pyroelectric energy generation of 140- μm -thick single crystal PMN-32PT capacitors poled in the [001] direction. The material was alternatively dipped into a cold silicone oil bath at 80°C and a hot one with temperature ranging from 130°C to 170°C. The electric field was cycled between 0.2 and 0.9 MV/m. A maximum energy density of 100 J/L/cycle was obtained at 0.049 Hz, corresponding to a power density of 4.92 W/L, for processes performed under quasiequilibrium conditions. McKinley *et al.* [25] performed the same procedure on [001]-poled PZN-5.5PT and generated 11.7 W/L for temperatures between 100°C and 190°C and electric field between 0 and 1.5 MV/m.

Furthermore, Lee *et al.* [33] studied the energy generation capabilities of relaxor ferroelectric 8/65/35 PLZT using the Olsen cycle. A maximum energy density of 888 J/L/cycle was generated at 0.0178 Hz, corresponding to a power density of 15.8 W/L, for operating temperatures between 25°C and 160°C and electric field cycled between 0.2 and 7.5 MV/m. This represents the largest energy density measured repeatedly over multiple cycles for a pyroelectric material.

Unfortunately, the power density achieved with 8/65/35 PLZT was limited by slow dipole relaxation during process 4–1, requiring the Olsen cycle to be operated at low frequencies. In fact, Kamba *et al.* [39] estimated that the energy barrier required to activate and reorient the polar nanodomains of 9.5/65/35 PLZT was lower than that of 8/65/35 PLZT by approximately 25%. A lower energy barrier may reduce the duration of the isoelectric

field processes 2–3 and 4–1 required for quasiequilibrium conditions to be reached. This would enable operation of the Olsen cycle at higher frequencies, therefore achieving larger power density from 9.5/65/35 PLZT than from 8/65/35 PLZT. Consequently, the present study intends to assess the power generation capabilities of relaxor ferroelectric 9.5/65/35 PLZT using the Olsen cycle.

D. 9.5/65/35 PLZT

The material investigated in this study is a quadratic electrostrictive ceramic composed of 9.5 mol.% lanthanum doped into a 65 mol.% lead zirconate and 35 mol.% titanate solid solution $[\text{Pb}_{0.905}\text{La}_{0.095}(\text{Zr}_{0.65}\text{Ti}_{0.35})_{0.976}\text{O}_3]$, denoted hereafter as 9.5/65/35 PLZT. The replacement of lead ions in PZT with lanthanum dopant counteracts the p-type conductivity of PZT and increases the electrical resistivity of PLZT materials by at least three orders of magnitude [40]. At room temperature, 9.5/65/35 PLZT features rhombohedral crystal symmetry and exhibits slim D-E loops [41], [42]. The material is a relaxor ferroelectric that undergoes complex phase transitions depending on the applied electric field, temperature, and frequency [36], [43]–[45]. It transforms from the paraelectric cubic to ergodic relaxor phase when cooled below the Burns temperature of about 350°C [39], [46]. Relaxor ferroelectrics possess large dielectric and piezoelectric constants in the ergodic relaxor phase resulting from distortion in the crystal structures caused by interactions between randomly oriented polar nanodomains [47]. The material transforms from the ergodic relaxor to the ferroelectric rhombohedral phase upon cooling below the Curie temperature T_{Curie} [44]. Note that the ferroelectric phase cannot be established in 9.5/65/35 PLZT upon cooling under zero bias fields [44], [45]. However, the ferroelectric phase can be induced from the ergodic relaxor phase by applying an external electric field E greater than a critical electric field $E_{\text{cr}}(T)$. This behavior was also observed in lead magnesium niobate $\text{Pb}(\text{Mg}_{1/2}\text{Nb}_{2/3})\text{O}_3$ relaxor [48]. Bobnar *et al.* [43] established that the ferroelectric phase could be formed in 9/65/35 PLZT under an applied electric field greater than $E_{\text{cr}} = 0.5$ MV/m and at temperatures above -23°C .

TABLE II. THICKNESS AND CROSS-SECTIONAL AREA OF SIX DIFFERENT 9.5/65/35 PLZT SAMPLES AND THEIR ELECTRODES INVESTIGATED IN THIS STUDY.

Sample	Electrode material	Thickness (μm)	Sample size ($\text{mm} \times \text{mm}$)	Electrode size ($\text{mm} \times \text{mm}$)
1	Au	250	10.07×9.75	9.51×8.55
2	Au	275	8.35×8.13	7.62×7.42
3	Au	500	7.57×6.94	5.28×4.70
4	Pt	250	7.43×7.02	6.35×6.28
5	Pt	250	7.43×7.02	6.19×6.50
6	Pt	190	7.43×7.02	6.10×7.34

The authors showed the dependence between T_{Curie} and E_{cr} for 9/65/35 PLZT in an E-T phase diagram [43]. Unfortunately, T_{Curie} and $E_{\text{cr}}(T)$ for the PLZT composition 9.5/65/35 have not been reported in the literature. Therefore, we will assume that the ferroelectric-relaxor phase transitions for 9.5/65/35 PLZT are similar to those for 9/65/35 PLZT reported in [43].

At temperatures above T_{Curie} , the isothermal D-E curves for 9/65/35 PLZT degenerate into narrow and linear loops [36]. Then, the remnant polarization $P_{\text{r}}(T)$, corresponding to the polarization under zero applied electric field, is negligibly small in the relaxor state with respect to its value in the ferroelectric state [49]. Therefore, the relaxor-ferroelectric phase transition is accompanied by a large change in electric displacement D . The Curie temperatures of 8/65/35 and 9.5/65/35 PLZT at 1 Hz and zero bias field were reported to be 113°C [50] and 65°C [51] at 1 kHz, respectively. This suggests that the 9.5/65/35 PLZT material should be operated over a narrower temperature range than 8/65/35 PLZT for optimum performance.

III. EXPERIMENTS

A. Samples

Hot isostatically pressed 9.5/65/35 PLZT ceramics with grain diameter around $5 \mu\text{m}$ were obtained from Aura Ceramics Inc. (New Hope, MN). Six samples with $10 \times 10 \text{ mm}$ rectangular cross-sections were cut from bulk blocks using a diamond blade. The samples were then polished by applying figure-eight strokes on sandpaper to achieve thicknesses ranging from 190 to 500 μm . Rectangular gold (Au) or platinum (Pt) electrodes were sputtered onto opposite faces of the samples about 1 to 2 mm from the edges. The electrode area was chosen to be smaller than the overall sample area to reduce electrical conduction around the sample edges [33]. Electrical wires were bonded to the electrodes using silver epoxy. Silicone conformal coating was also applied to both faces of the samples and cured at 65°C for one hour to increase their dielectric strength [52]. Table II summarizes the thickness and cross-sectional area of the six 9.5/65/35 PLZT samples investigated in this study.

B. Electrical and Thermal Subsystems

The electrical subsystem used to measure isothermal D-E loops and to perform the Olsen cycle consisted of a

modified Sawyer-Tower bridge circuit. It was used to apply the required electric field across the pyroelectric element and to measure the charge Q across the electrode surfaces. Details of the circuit used in the present study were provided in previous studies [24], [26], [33] and need not be repeated.

The thermal subsystem consisted of two beakers containing dielectric fluids Dow Corning (Midland, MI) 100-cSt silicone oil or Fluorinert FC-70 (3M, St. Paul, MN) maintained at T_{cold} and T_{hot} by temperature-controlled hot plates [24], [26], [33]. Dow Corning oil was used for temperatures above room temperature. Fluorinert was used for temperatures near 0°C . Each beaker contained a magnetic stirrer to ensure uniform temperature. For temperatures below room temperature, the cold beaker was placed in an ice bath. Oil temperatures were monitored using K-type thermocouples.

C. Experimental Procedure

1) *Isothermal D-E Loops*: Isothermal bipolar D-E loops were measured by immersing the samples in silicone oil baths maintained at temperatures $T_{\text{cold}} = 23^{\circ}\text{C}$ and $T_{\text{hot}} = 140^{\circ}\text{C}$. The D-E loops were collected by applying a continuous triangular voltage signal across the sample at 0.1 Hz. This frequency corresponded to that of the isothermal electric field changes occurring in processes 1–2 and 3–4 of the Olsen cycle. D-E loops were measured with increasing electric field span. The applied electric field E_{H} was increased in 1.0 MV/m increments from 3.0 to 6.0 MV/m and then in 0.25 MV/m increments as E_{H} approached 6.75 MV/m.

2) *Olsen Cycle*: The Olsen cycle was performed on all samples under various electric fields, temperatures, and frequencies to investigate their respective effects on the energy and power generated. The energy density N_{D} generated by the Olsen cycle and given by (2) was numerically estimated using the trapezoidal rule. The power density was computed according to (3). Preliminary tests (not shown) indicated that the energy density N_{D} reached a maximum for low electric field $E_{\text{L}} = 0.2 \text{ MV/m}$. Therefore, all measurements reported in the remainder of this study correspond to $E_{\text{L}} = 0.2 \text{ MV/m}$. However, the high electric field E_{H} was varied from 2.0 to 6.75 MV/m. Similarly, the cold source temperature T_{cold} was either 3 or 23°C and the hot source temperature T_{hot} was equal to

140°C. As discussed earlier, decreasing T_{cold} should result in a larger energy density. Between T_{cold} and $T_{\text{hot}} \geq T_{\text{Curie}}$, the 9.5/65/35 PLZT samples underwent a phase transition from ferroelectric to ergodic relaxor accompanied by a significant decrease in electric displacement D . Therefore, large energy densities could be achieved near the ferroelectric-relaxor phase transition temperature T_{Curie} reported to be below 0°C [53]. However, the temperature T_{cold} was physically limited to 3°C. Between $T_{\text{cold}} = 3^\circ\text{C}$ and $T_{\text{hot}} = 140^\circ\text{C}$, the 9.5/65/35 PLZT samples featured a significant difference in electric displacement D but only in the presence of an electric field.

Finally, the overall cycle frequency was defined as $f = (\tau_{12} + \tau_{23} + \tau_{34} + \tau_{41})^{-1}$ where τ_{ij} corresponds to the duration of process $i-j$. It was varied between 0.025 and 0.16 Hz by changing the duration of the isoelectric field heating process 2-3 and cooling process 4-1 denoted by τ_{23} and τ_{41} , respectively. For example, the times τ_{23} and τ_{41} varied between ~ 1 and ~ 10 s. However, the durations of the isothermal processes 1-2 (τ_{12}) and 3-4 (τ_{34}) were kept constant at ~ 1.5 s. Quasiequilibrium conditions were achieved when the electric displacement reached steady state, i.e., $(\partial D/\partial T) = 0$, during processes 2-3 and 4-1 before the electric field was varied in processes 3-4 and 1-2, respectively. Operating the Olsen cycle under quasiequilibrium conditions resulted in the maximum energy density [25]. On the other hand, to maximize the power density, the Olsen cycle was performed at higher frequencies by reducing the duration of isoelectric field processes 2-3 and 4-1.

IV. RESULTS AND DISCUSSION

A. Isothermal D-E Loops and Olsen Cycle

Fig. 2 presents typical isothermal bipolar D-E loops measured with sample 4 at $T_{\text{cold}} = 23^\circ\text{C}$ and $T_{\text{hot}} = 140^\circ\text{C}$ between 0.2 and 4.0 MV/m at 0.1 Hz. The sample exhibited the slim-loop relaxor behavior at 140°C typically observed in $x/65/35$ PLZT ceramics with $x = 9$ to 10% [9]. Note that the bipolar D-E loops were similar among samples for any given temperature. Upon a decrease in temperature below T_{Curie} , the remnant polarization of relaxor ferroelectric materials typically increases from around zero in the relaxor state to finite values in the ferroelectric state. The Curie temperature was reported to be between -50°C and 0°C for 9.5/65/35 PLZT [53]. Fig. 2 shows that 9.5/65/35 PLZT did not exhibit remnant polarization at 23°C or 140°C, indicating that the material remained in the relaxor state in this temperature range. However, the material became polarized under an applied electric field, and then an absolute difference in electric displacement was observed.

Moreover, Fig. 2 depicts an experimental Olsen cycle performed under quasi-equilibrium conditions at $f = 0.038$ Hz, for the same sample, at temperatures between $T_{\text{cold}} = 23^\circ\text{C}$ and $T_{\text{hot}} = 140^\circ\text{C}$ and electric fields cycled

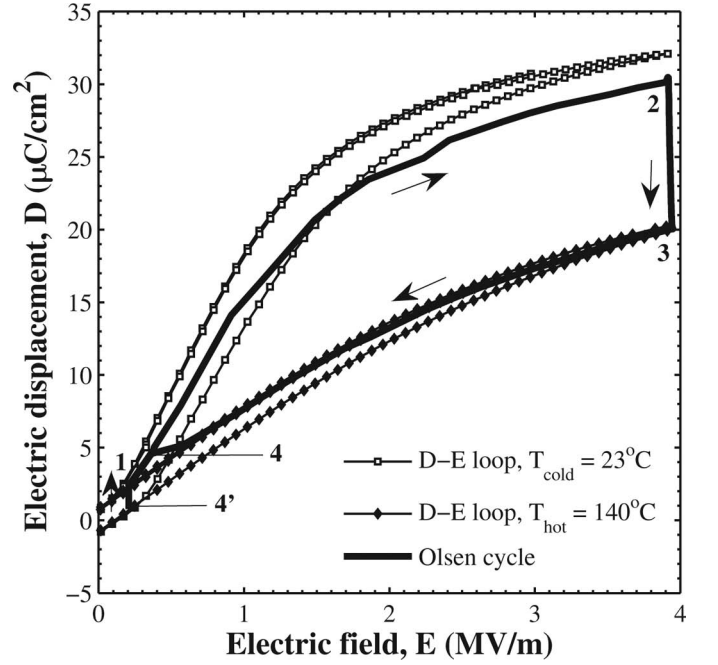


Fig. 2. D - E diagram of isothermal bipolar D - E loops and Olsen cycle performed under quasiequilibrium conditions for a 250- μm -thick 9.5/65/35 PLZT sample (sample 4). The temperatures T_{cold} and T_{hot} were 23°C and 140°C, respectively; the electric field was cycled between $E_L = 0.2$ MV/m and $E_H = 4.0$ MV/m. The Olsen cycle was vertically displaced to coincide with the isothermal D - E curve at T_{hot} .

between $E_L = 0.2$ MV/m and $E_H = 4.0$ MV/m. Process 3-4 follows the decreasing electric field path of the isothermal D-E loop at T_{hot} . However, process 1-2 did not follow the increasing electric field path of the isothermal D-E loop at T_{cold} . The fact that the Olsen cycle did not span the electric displacement between the isothermal bipolar D-E loop corresponding to T_{cold} may be attributed to the existence of mixed ferroelectric and ergodic relaxor phases [3], [54] when the applied electric field increased from E_L to $E_{\text{cr}}(T)$ during the Olsen cycle. These phases co-exist likely because of slow stabilization of the ferroelectric phase from the relaxor phase caused by parasitic interactions between defects and polar nanoregions [54].

Furthermore, note that points 4 and 4' of the Olsen cycle do not coincide. The offset was attributed to leakage current across the PLZT ceramic often observed at high temperatures and/or large electric fields [15], [26], [38], [55]. Additionally, the change in electric displacement was negligibly small in isoelectric cooling process 4'-1 from $T_{\text{cold}} = 23^\circ\text{C}$ and $T_{\text{hot}} = 140^\circ\text{C}$, indicating that this process can be performed on 9.5/65/35 PLZT nearly instantaneously. This was made possible by operating at temperatures corresponding to the relaxor phase with small remnant polarization. Indeed, for 8/65/35 PLZT, this was a long process in the Olsen cycle [33] caused by slow dipole-dipole relaxation [56].

B. Effect of High Electric Field E_H

Fig. 3 shows (a) the energy density and (b) the power density generated by samples 1 to 4 under quasi-equilib-

rium conditions for cycle frequencies between 0.029 and 0.057 Hz. The high electric field E_H ranged from 2.0 to 6.75 MV/m while the low electric field E_L was maintained at 0.2 MV/m. The cold and hot source temperatures were 23°C and 140°C, respectively. Each data point corresponds to the average over five Olsen cycles; the error bar corresponds to two standard deviations or 95% confidence interval. Fig. 3 indicates that the largest sample variation in energy density was found for $E_H = 3.0$ MV/m with a maximum relative difference among samples of 23%. Meanwhile, sample variability was the lowest for $E_H = 5.0$ MV/m, with a maximum relative difference among samples of 6%. These results establish the consistency and repeatability of experimental measurements not only from one cycle to another but also from one sample to another.

Fig. 3(a) also indicates that raising the electric field span ($E_H - E_L$) resulted in larger energy densities. For example, the energy density generated by a 250- μm -thick sample increased by 38.4% from 240 to 332 J/L/cycle when the high electric field E_H increased from 3.0 to 4.0 MV/m. However, the maximum value of E_H was limited by the samples' dielectric breakdown. For example, beyond an electric field threshold, cracks formed within the sample. The formation of cracks may be attributed to mechanical stresses in the material along the grain boundaries because of spatially variant electric fields causing preferential domain wall motion [57]. Microcracks may then propagate along the grain boundaries of the sample under the cyclic electric field loading. This phenomenon was previously observed in 9.4/65/35 PLZT for applied electric fields around 0.3 MV/m [58]. Additionally, the crack lengths of Vicker's indentation test under zero field have been shown to increase with increasing temperature [35]. Thus, the combination of cycling high temperature and high electric field caused the samples to fracture.

C. Effect of Sample Thickness b

The dielectric breakdown strength of ceramics was reported to increase with decreasing sample thickness [59]. Consequently, the effect of sample thickness on the energy and power densities was investigated with samples 1 to 3 whose thicknesses were 250, 275, and 500 μm , respectively. Fig. 3 shows that a reduction in sample thickness enabled larger electric fields to be applied across the sample without causing electrical breakdown. In fact, samples with thickness 500 μm (sample 3) and 250 μm (sample 1) had electric field breakdown of 6.0 and 6.75 MV/m, respectively. This resulted in a maximum energy density of 427.8 and 636.9 J/L/cycle, for samples 1 and 3, corresponding to a power density of 13.6 and 22.7 W/L, respectively. The increase in breakdown field can be explained by the presence of fewer domains in thinner samples. Therefore, thinner films had fewer grain boundaries and lower occurrences of crack formation. This, in turn, enabled larger energy and power densities to be achieved.

Furthermore, using PLZT thin films offers advantages including 1) a substantial reduction in the applied voltage

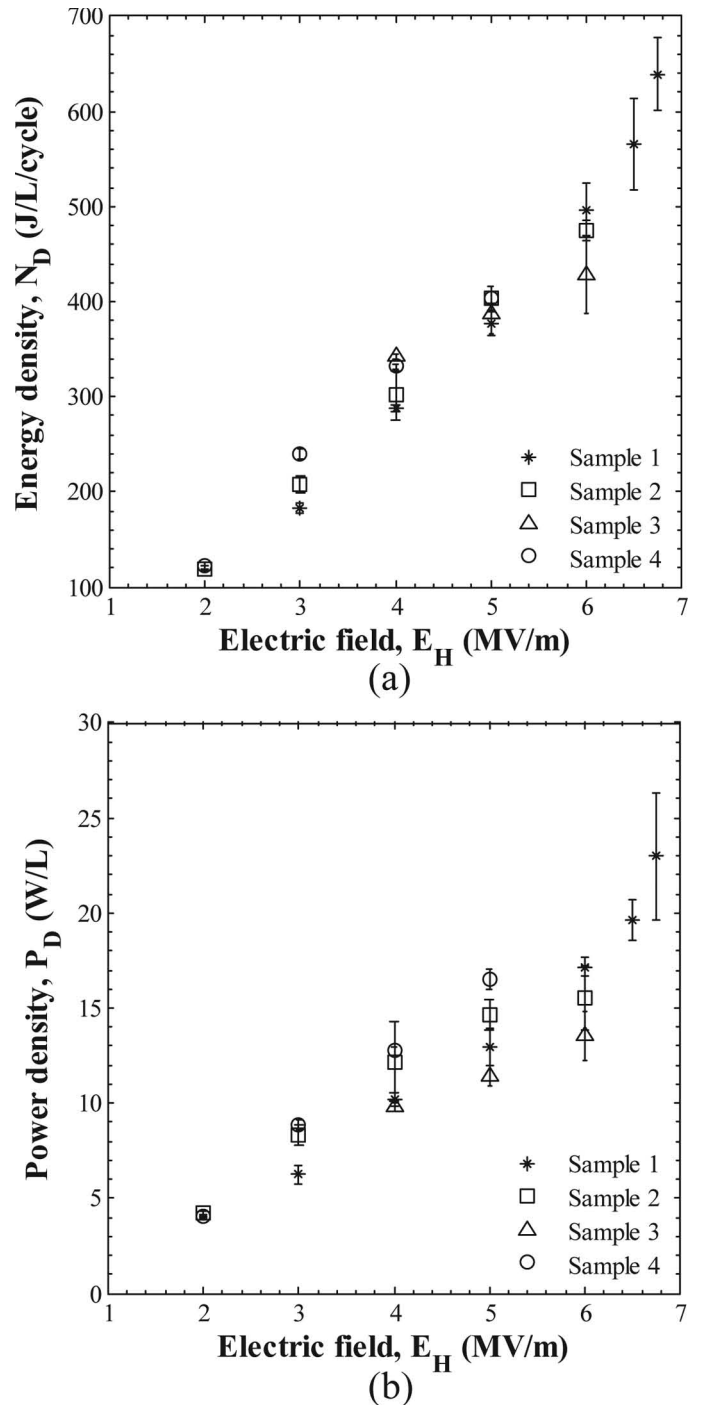


Fig. 3. (a) Energy density and (b) power density generated by 9.5/65/35 PLZT (samples 1 to 4) as a function of high electric field E_H between 2.0 and 6.75 MV/m under quasiequilibrium conditions. The low electric field E_L was 0.2 MV/m; the cold and hot source temperatures were $T_{\text{cold}} = 23^\circ\text{C}$ and $T_{\text{hot}} = 140^\circ\text{C}$, respectively.

delivered to the electrical circuit during the Olsen cycle, 2) faster thermal response, and 3) smaller size and lower weight for easier integration into devices. For example, as the specimen thickness was reduced from 500 μm (sample 3) to 250 μm (sample 1), the power density was found to increase by 26% from 13.56 to 17.15 W/L for high electric field $E_H = 6.0$ MV/m. This may be explained by a reduction in the thermal time constant associated with thinner

films and the increase in cycle frequency f from 0.030 to 0.035 Hz. In addition, only 12 V applied across a 20- μm thin PLZT film would be required to achieve an electric field of 6.0 MV/m instead of 1140 V required across a 190- μm -thick sample (sample 6).

D. Effect of Electrode Material

Large mechanical stresses may be induced at the interface of two distinct materials subjected to large temperature variations if their thermal expansion coefficients feature large mismatch. Thus, the electrode material may affect the performance of pyroelectric materials. To investigate this effect, Pt or Au electrodes of identical thickness were deposited on 9.5/65/35 PLZT samples. The thermal expansion coefficient in the thickness direction of 9.5/65/35 PLZT, platinum, and gold were reported to be equal to 5.4 $\mu\text{m}/\text{m}/^\circ\text{C}$ [41], 8.8 $\mu\text{m}/\text{m}/^\circ\text{C}$ [60], and 14.2 $\mu\text{m}/\text{m}/^\circ\text{C}$ [60], respectively. Fig. 3(b) indicates that 9.5/65/35 PLZT samples of the same thickness with gold (sample 1) or platinum (sample 4) electrodes had similar power density for all frequencies. However, the samples with Pt electrodes (samples 4–6) were capable of sustaining larger temperature swings ($T_{\text{hot}} - T_{\text{cold}}$) than the samples with Au electrodes (samples 1–3). These results establish that it is important to utilize the electrode material which has the closest thermal expansion coefficient to that of the selected pyroelectric material. This may reduce the susceptibility of a pyroelectric material to thermomechanical breakdown upon repeated cycling with large temperature differences.

E. Effect of Cold Source Temperature T_{cold}

As previously discussed, increasing the difference between T_{cold} and T_{hot} should result in larger energy density. Fig. 4 shows (a) the energy density and (b) the power density generated by samples 4 and 5 as a function of high electric field E_{H} and frequencies between 0.033 and 0.057 Hz corresponding to quasiequilibrium. The low electric field was set as $E_{\text{L}} = 0.2$ MV/m. The cold source temperature T_{cold} was maintained at 23 $^\circ\text{C}$ (for sample 4) or 3 $^\circ\text{C}$ (for sample 5). The hot source temperature was fixed at 140 $^\circ\text{C}$. Fig. 4 establishes that for a given high electric field E_{H} , both the energy and power densities increased by an average of 44.6 J/L/cycle (16.7%) and 6.6 W/L (67%), respectively, as the cold source temperature T_{cold} was reduced from 23 $^\circ\text{C}$ to 3 $^\circ\text{C}$. Note that sample 4 broke before we could perform tests for E_{H} larger than 5.0 MV/m. The increase in energy density was attributed to the increase in electric displacement span ΔD as T_{cold} was lowered. In other words, more free charges were collected at the electrode surface as T_{cold} decreased from 23 $^\circ\text{C}$ to 3 $^\circ\text{C}$.

Moreover, Lee *et al.* [33] observed that as T_{cold} was lowered, the energy density generated by 8/65/35 PLZT increased but the power density decreased. This was explained by the significant increase in time required for isoelectric field cooling process 4–1 to operate under quasi-

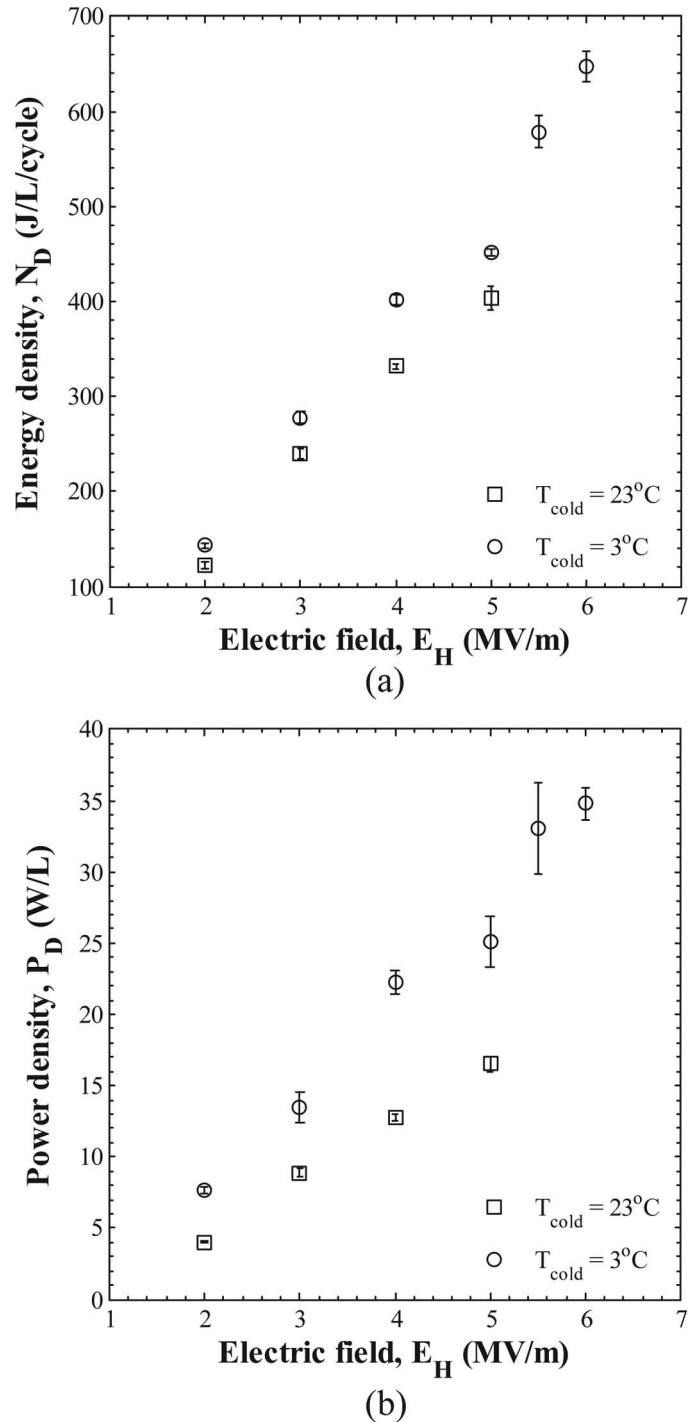


Fig. 4. (a) Energy density and (b) power density generated by 9.5/65/35 PLZT for $T_{\text{cold}} = 23^\circ\text{C}$ (sample 4) or 3°C (sample 5) as a function of high electric field E_{H} under quasiequilibrium conditions. The low electric field E_{L} was 0.2 MV/m and the hot source temperature $T_{\text{hot}} = 140^\circ\text{C}$.

equilibrium conditions. In contrast, this process was short in 9.5/35/65 PLZT samples operating in the relaxor phase above T_{Curie} . A reduction in cold source temperature from 23 $^\circ\text{C}$ to 3 $^\circ\text{C}$ had no significant effect on the quasiequilibrium cycle period. As a result, the power density of 9.5/65/35 PLZT increased as the cold source temperature T_{cold} was reduced from 23 $^\circ\text{C}$ to 3 $^\circ\text{C}$. Note that a reduction of T_{cold} from 3 $^\circ\text{C}$ to -50°C would increase the rem-

nant polarization of 9.5/65/35 PLZT from around 0.01 to 0.11 C/m² [53]. This could result in larger energy density. However, the duration of isoelectric cooling process 4–1 would no longer be short because of a significant increase in dipole relaxation time for relaxor ferroelectric materials undergoing relaxor to ferroelectric phase transition. Therefore, we speculate that decreasing T_{cold} from 3°C to below 0°C will result in a lower power density.

F. Effect of Cycle Frequency f

Fig. 5 plots both the energy and the power densities obtained with sample 4 as a function of cycle frequency for $E_L = 0.2$ MV/m and $E_H = 5.0$ MV/m. The cold and hot temperatures were $T_{\text{cold}} = 23^\circ\text{C}$ and $T_{\text{hot}} = 140^\circ\text{C}$, respectively. The durations of the isothermal processes 1–2 (τ_{12}) and 3–4 (τ_{34}) were set at ≈ 1.5 s. Meanwhile, the duration of isoelectric field processes 2–3 (τ_{23}) and 4–1 (τ_{41}) were the same and ranged from about 1 to 10 s. The four different processes in the Olsen cycle performed at frequencies below 0.057 Hz corresponded to quasiequilibrium conditions.

Fig. 5 shows that, under these conditions, the energy density reached a maximum of 441 J/L/cycle at frequencies below 0.057 Hz and then decreased with increasing cycle frequency. Unfortunately, for frequencies below 0.057 Hz, the energy density decreased because of excessive leakage current. At such low frequencies, the duration of isoelectric field process 2–3 was longer than the time required for the electric displacement to reach steady state and this provided an opportunity for charges at the surface of the PE to conduct through its body. Indeed, leakage current increases with increasing time at which the

PE operates at high electric fields. However, as the cycle frequency increased beyond 0.057 Hz, the energy density decreased because of a reduction in electric displacement span ΔD because the processes were not performed under quasiequilibrium conditions.

Additionally, Fig. 5 indicates that under these conditions, the power density P_D reached a maximum of 34.7 W/L at 0.11 Hz. Performing the Olsen cycle at frequencies greater than 0.11 Hz led to a smaller power output. This was due to the fact that the dipole realignment and phase transitions occurring during the isoelectric field processes 2–3 and 4–1 may not have time to be complete at higher frequencies. Moreover, although the energy density was smaller at 0.11 Hz than at 0.057 Hz, the smaller cycle time resulted in a larger power density. Overall, the maximum power density can be achieved by considering the expression $P_D = N_D(f)f$. It is achieved through a compromise between a small cycle time (large f) and large electric displacement span ΔD with minimal leakage current (large N_D).

Fig. 6 plots the power density generated by sample 5 as a function of cycle frequency between 0.10 and 0.16 Hz. The low electric field E_L was set as 0.2 MV/m, whereas the high electric field E_H was set as either 5.0, 5.5, or 6.0 MV/m. The cold and hot source temperatures were $T_{\text{cold}} = 3^\circ\text{C}$ and $T_{\text{hot}} = 140^\circ\text{C}$, respectively. Preliminary tests (not shown) demonstrated that the change in electric displacement was negligibly small during process 4–1. Therefore, the duration of process 4–1 (τ_{41}) was set to be short at ≈ 1 s. Durations of processes 1–2 (τ_{12}) and 3–4 (τ_{34}) were kept identical and constant at ≈ 1.5 s. However, the duration of process 2–3 (τ_{23}) was varied from ~ 1 to 4 s. Fig. 6 indicates that the peak power density increased with increasing high electric field E_H . The increase in electric field E_H in combination with the increase in rate of electric field change led to an increase in the enclosed 1–2–3–4 area (N_D), as shown in Fig. 1, without requiring a decrease in the cycle frequency f . In addition, the decrease in the duration of process 4–1 (τ_{41}) from ~ 1 to 10 s to ~ 1 s resulted in an increase in the peak power frequency from 0.11 to 0.14 Hz.

Zhu *et al.* [23] studied the effect of time rate of change of the electric field on the energy density generated by [110]-poled PZN-4.5PT by performing the Olsen (or Ericsson) cycle. The authors reported that the energy density can be increased by decreasing the duration of process 1–2 and by increasing the duration of process 3–4 in the Olsen cycle. Moreover, a uniform increase in the time rate of change of electric field for both processes 1–2 and 3–4 resulted in a nonlinear decrease in energy density [23]. However, the energy density remained nearly constant for rates of electric field change between 0.08 and 8.0 MV/m/s [23]. Consequently, it was assumed that the power densities presented in Fig. 6 were not influenced by variations in the time rate of change in electric field from $E_L = 0.2$ MV/m to $E_H = 5.0, 5.5,$ or 6.0 MV/m, corresponding to similar time rates of 3.20, 3.53, and 3.87 MV/m/s, respectively.

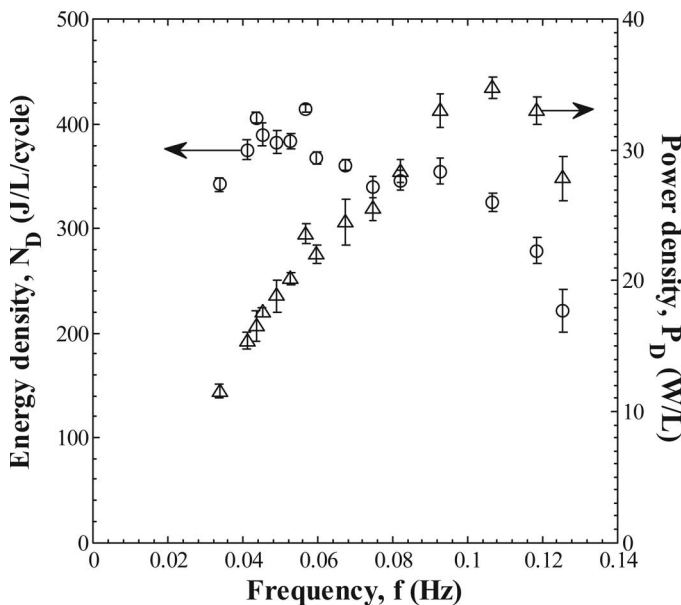


Fig. 5. Energy and power densities generated by 9.5/65/35 PLZT (sample 4) as a function of cycle frequency. The cold and hot source temperatures were $T_{\text{cold}} = 23^\circ\text{C}$ and $T_{\text{hot}} = 140^\circ\text{C}$, respectively. The low electric field E_L was 0.2 MV/m and the high electric field E_H was fixed at 5.0 MV/m.

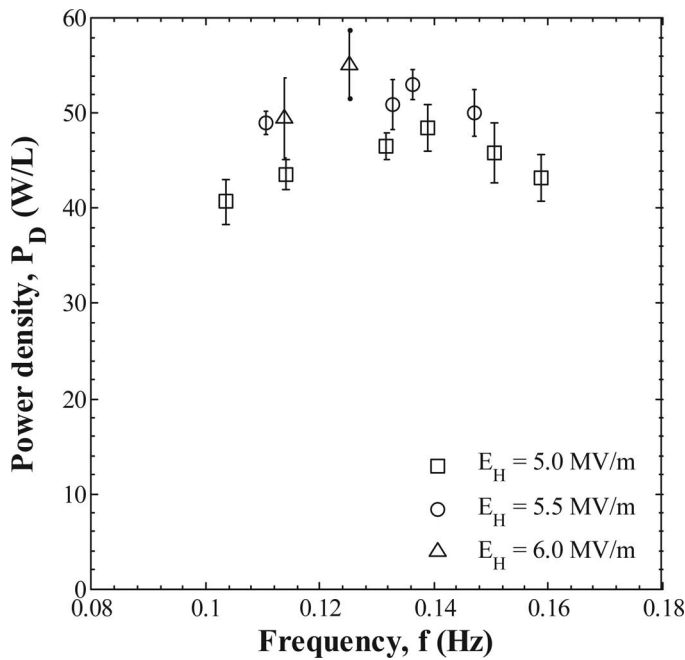


Fig. 6. Power density generated by 9.5/65/35 PLZT (sample 5) as a function of cycle frequency. The cold and hot source temperatures were $T_{\text{cold}} = 3^\circ\text{C}$ and $T_{\text{hot}} = 140^\circ\text{C}$, respectively. The low electric field E_L was 0.2 MV/m. The high electric field E_H was equal to 5.0, 5.5, or 6.0 MV/m.

G. Maximum Power Density

Fig. 6 also shows that a maximum power density of 55.26 ± 7.99 W/L was obtained with sample 5 at 0.125 Hz, corresponding to an energy density of 441.0 ± 29.4 J/L/cycle. The cold and hot source temperatures were $T_{\text{cold}} = 3^\circ\text{C}$ and $T_{\text{hot}} = 140^\circ\text{C}$, respectively; the electric field was cycled between $E_L = 0.2$ MV/m and $E_H = 6.0$ MV/m. Fig. 7 presents four consecutive Olsen cycles on the D - E diagram corresponding to this maximum power density. The Olsen cycles did not follow a smooth path between E_L and E_H during processes 1-2 and 3-4 in the D - E diagram, indicating that the processes were not performed under quasiequilibrium conditions. Fig. 7 also shows that the D - E paths of the Olsen cycles were not closed because points 4 and 4' did not coincide. This indicates that leakage current was observed across the PLZT ceramic at high temperatures and/or large electric fields [15], [26], [38], [55].

The maximum power density of 55.3 W/L generated by 9.5/65/35 PLZT is an improvement over the 33.9 W/L produced by PZST ceramic [48], 24.3 W/L obtained by [110] PZN-4.5PT single crystal [22], 15.8 W/L achieved by 8/65/35 PLZT ceramic [33], 11.7 W/L generated by [001] PZN-5.5PT single crystal [25], and 4.92 W/L produced by [001] PMN-32PT single crystal. The reader is referred to Table I for the experimental conditions (T_{cold} , T_{hot} , E_L , E_H , f) used in these various studies. In addition, the power density produced by 9.5/65/35 PLZT is comparable to the 58 W/L generated by 60/40 P(VDF-TrFE) polymer for a similar temperature range [26]. However, using 9.5/65/35 PLZT offers advantages over 60/40 P(VDF-TrFE) in that

it 1) possesses low leakage current, 2) does not require electrical poling before performing the Olsen cycle, and 3) requires smaller electric field E_H and applied voltages in the Olsen cycle (Table I).

H. Sample Durability

Pyroelectric materials for energy harvesting applications are meant to be integrated into devices where the Olsen cycle is expected to be performed for a very large number of cycles. However, large mechanical stresses are thermally and electrically induced within the samples under repeated thermal and electrical loading [61]. The excessive stresses may initiate the development of microcracks along the domain boundaries. These cracks lead to the gradual degradation of the material performance.

Therefore, a preliminary fatigue test was performed on sample 6 to assess its durability. Sample 6 was subjected to around 85 successive Olsen cycles with operating temperatures between 23 and 140°C and electric field cycled between 0.2 and 5.0 MV/m. Fig. 8(a) plots the energy and power densities generated by sample 6 as a function of cycle number. Five-point moving averages are also plotted to guide the eye. A decrease in the energy and power densities was observed at around cycle 72, possibly marking the onset of stress-induced sample cracking. Fig. 8(b) compares the 1st, 10th, and 82nd Olsen cycles on a D - E diagram. Between cycle 1 and cycle 82, the electric displacement span featured similar behavior at high electric

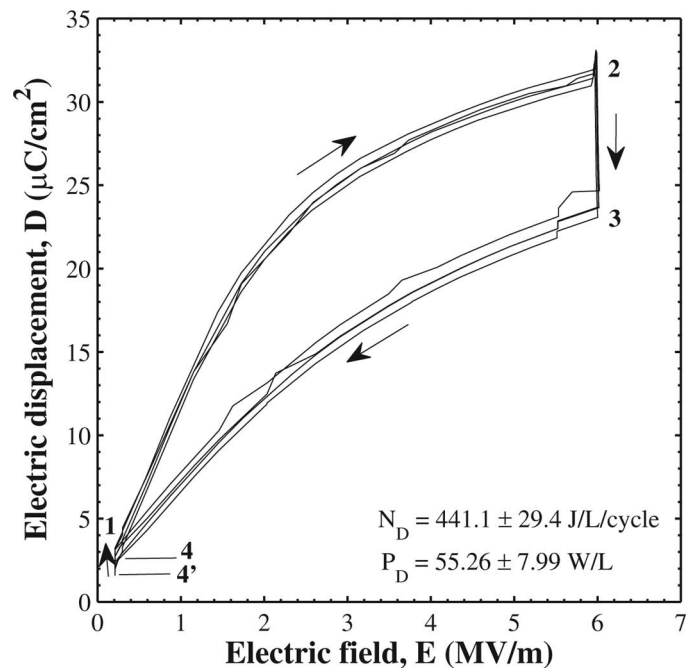


Fig. 7. Electric displacement versus electric field diagram containing four experimental Olsen cycles (sample 5). The electric field was cycled between 0.2 and 6.0 MV/m. The cold source temperature T_{cold} and hot source temperature T_{hot} were 3°C and 140°C , respectively. The average power density over four cycles was 55.26 W/L at 0.125 Hz, corresponding to the largest power density generated by 9.5/65/35 PLZT in this study.

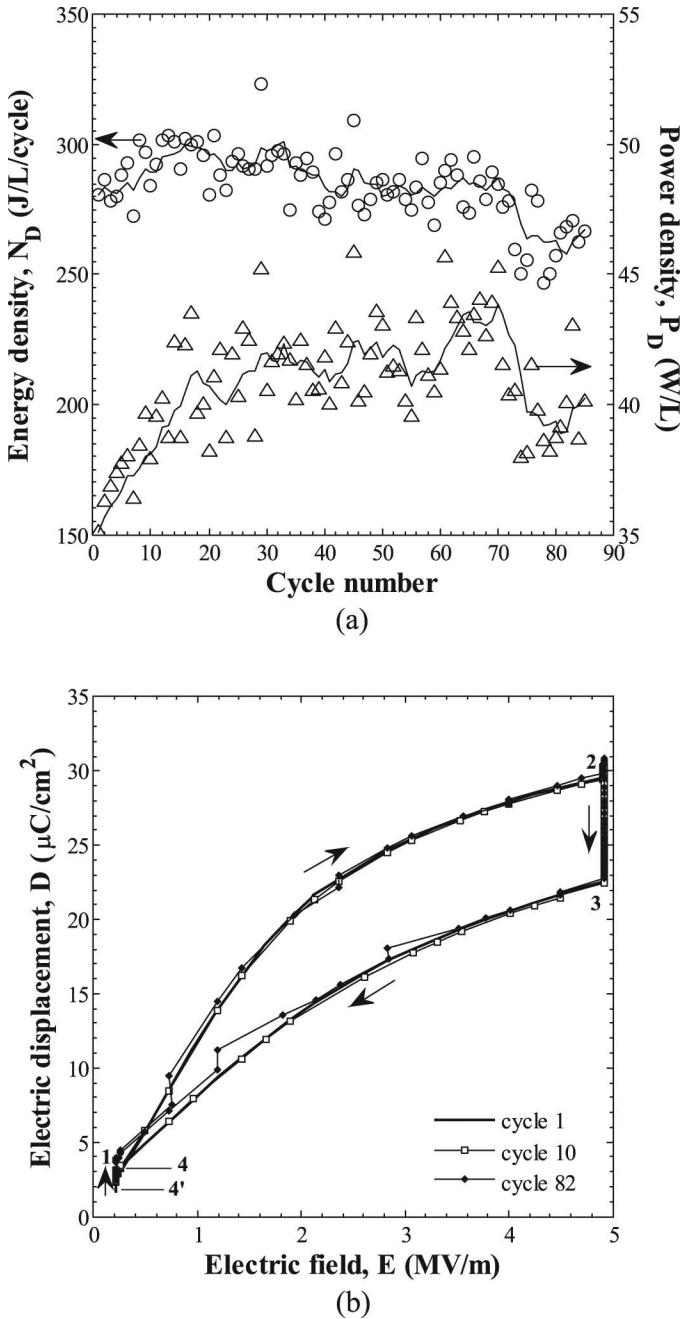


Fig. 8. (a) Energy and power densities generated by 9.5/65/35 PLZT (sample 6) as a function of cycle number. Solid lines represent the 5-point moving average. The cold and hot source temperature was $T_{\text{cold}} = 23^\circ\text{C}$ and $T_{\text{hot}} = 140^\circ\text{C}$, respectively. The low and high electric field were $E_L = 0.2$ MV/m and $E_H = 5.0$ MV/m. The average cycle frequency was 0.144 ± 0.008 Hz. Cracks began to develop within the sample after about 72 successive cycles. (b) D - E diagrams of the 1st, 10th, and 82nd Olsen cycles collected using sample 6.

fields. However, it is apparent that the electric displacement span decreased at low electric fields. This behavior is consistent with the fact that crack volume is directly correlated with polarization loss [62]. The latter can be explained by the concentration of defects present in microcracks limiting domain wall mobility [63]. Thus, the number of dipoles that can switch orientation under electric field cycling is reduced, corresponding to a decrease in po-

larization [63]. The degradation of performance with cycle number suggests that strategies to improve the electro-mechanical breakdown strength of PLZT ceramics should be explored and implemented in future studies to enhance the material and device reliability.

I. Discussion

The power density achieved in this study could be further increased by fabricating the samples into single or multilayer capacitors with thicknesses on the order of micrometers or less to increase the applied electric field without sample failure [41] and to promote faster thermal response. The power generation capabilities of these thin film PLZTs should be compared with their respective bulk counterparts.

Moreover, the power output of devices using conduction [34], convection [28], or radiation [27] could be advantageously enhanced by employing a multistaging technique envisioned by Olsen *et al.* [10]. This technique consists of placing pyroelectric materials in the order of increasing T_{Curie} between the cold and the hot sources. For example, the 9.5/65/35 PLZT material with Curie temperature around 65°C [51] at zero electric field can be included in the same multistage device as 8/65/35 PLZT and 6/65/35 PLZT with Curie temperatures of 113°C [50] and 240°C [4], respectively.

Furthermore, the PLZT compositions along the morphotropic phase boundary ($x/52/48$) possess a large dielectric constant, remnant polarization, and piezoelectric coefficient because of strong electromechanical coupling [4]. Therefore, the energy and power generation capabilities of these PLZT systems should be evaluated.

Finally, Fig. 1 indicates that a large energy density is inherent in materials with large remnant polarization at temperature T_{cold} . In fact, the remnant polarizations of 2/65/35 PLZT and 8/65/35 PLZT at room temperature were reported to be 39 and 35 C/m^2 , respectively [4]. This suggests that energy density generated by 2/65/35 PLZT could be larger than the 888 J/L/cycle achieved with 8/65/35 PLZT [33]. However, the Curie temperature of $x/65/35$ PLZT increases as the lanthanum doping level x decreases [4]. In fact, $T_{\text{Curie}} = 320^\circ\text{C}$ [4] for the composition 2/65/35 PLZT, and unfortunately it may be prohibitively high for waste heat harvesting devices.

V. CONCLUSION

This study was concerned with experimental measurements of the energy and power densities generated by subjecting electrostrictive 9.5/65/35 PLZT to the Olsen cycle. A maximum energy density of 637 ± 20 J/L/cycle was generated under quasiequilibrium conditions with a 250- μm -thick sample and operating temperatures $T_{\text{cold}} = 3^\circ\text{C}$ and $T_{\text{hot}} = 140^\circ\text{C}$ while the electric field was cycled from $E_L = 0.2$ to $E_H = 6.0$ MV/m. A maximum power density of 55 ± 8 W/L was obtained at 0.125 Hz for the

same specimen thickness, operating temperatures, and imposed electric fields. To the best of our knowledge, this power density is the largest achieved among pyroelectric single crystals and ceramics using the Olsen cycle. The dielectric strength, and therefore the energy and power densities, of the material increased when the sample thickness decreased from 500 to 250 μm . Moreover, the electrode material was found to have no significant effect on the energy and power densities when the samples were subject to the same operating temperatures and electric fields. However, samples with electrode material possessing thermal expansion coefficients similar to that of PLZT were capable of withstanding larger temperature swings. The maximum applied electric field and temperature swings of the material were physically limited by the samples' dielectric breakdown and thermoelectromechanical stress leading to cracks. In addition, a fatigue test showed that the power generation gradually degraded when the sample was subject to repeated thermoelectrical loading. Future work should focus on identifying pyroelectric materials featuring high electromechanical breakdown strength and large electric displacement span.

REFERENCES

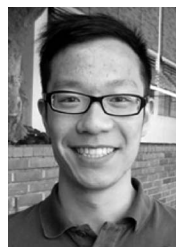
- [1] Lawrence Livermore National Laboratory. (2011, Sep.) U.S. Energy flow trends—2009. [Online]. Available: <https://publicaffairs.llnl.gov/news/energy/energy.html#2009>
- [2] M. Lallart, P. J. Cottinet, D. Guyomar, and L. Lebrun, "Electrostrictive polymers for mechanical energy harvesting," *J. Polym. Sci., B, Polym. Phys.*, vol. 50, no. 8, pp. 523–535, 2012.
- [3] A. Safari, R. K. Panda, and V. F. Janas, "Ferroelectricity: Materials, characteristics, and applications," *Key Eng. Mater.*, vol. 122–124, pp. 35–71, 1996.
- [4] G. H. Haertling and R. C. Buchanan, Eds. *Ceramic Materials for Electronics: Processing, Properties, and Applications*. New York, NY: Marcel Dekker, 1991.
- [5] P. C. A. Hammes and P. P. L. Regtien, "An integrated infrared sensor using the pyroelectric polymer PVDF," *Sens. Actuators A*, vol. 32, no. 1–3, pp. 396–402, 2008.
- [6] S. L. Swartz, "Topics in electronic ceramics," *IEEE Trans. Electr. Insul.*, vol. 25, no. 5, pp. 935–987, 1990.
- [7] I. H. Pratt and S. Firestone, "Fabrication of RF-sputtered barium titanate thin films," *J. Vac. Sci. Technol.*, vol. 8, no. 1, pp. 256–260, 1971.
- [8] G. L. Brennecke, J. F. Ihlefeld, J.-P. Maria, B. A. Tuttle, and P. G. Clem, "Processing technologies for high-permittivity thin films in capacitor applications," *J. Am. Ceram. Soc.*, vol. 93, no. 12, pp. 3935–3954, 2010.
- [9] R. B. Olsen and D. A. Bruno, "Pyroelectric conversion materials," in *Proc. 21st Intersociety Energy Conversion Engineering Conf., American Chemical Society*, 1986, pp. 89–93.
- [10] R. B. Olsen, D. A. Bruno, and J. M. Briscoe, "Cascaded pyroelectric energy converter," *Ferroelectrics*, vol. 59, no. 3–4, pp. 205–219, 1984.
- [11] R. B. Olsen, D. A. Bruno, and J. M. Briscoe, "Pyroelectric conversion cycles," *J. Appl. Phys.*, vol. 58, no. 12, pp. 4709–4716, 1985.
- [12] R. B. Olsen, D. A. Bruno, J. M. Briscoe, and W. F. Butler, "A pyroelectric energy converter which employs regeneration," *Ferroelectrics*, vol. 38, no. 1–4, pp. 975–978, 1981.
- [13] R. B. Olsen, "Ferroelectric conversion of heat to electrical energy—A demonstration," *J. Energy*, vol. 6, pp. 91–95, 1982.
- [14] R. B. Olsen and D. D. Brown, "High-efficiency direct conversion of heat to electrical energy related pyroelectric measurements," *Ferroelectrics*, vol. 40, no. 1–2, pp. 17–27, 1982.
- [15] L. Kouchachvili and M. Ikura, "Improving the efficiency of pyroelectric conversion," *Int. J. Energy Res.*, vol. 32, no. 4, pp. 328–335, 2008.
- [16] L. Kouchachvili and M. Ikura, "High performance P(VDF-TrFE) copolymer for pyroelectric conversion," U.S. Patent 7323506, Jan. 29, 2008.
- [17] M. Ikura, "Conversion of low-grade heat to electricity using pyroelectric copolymer," *Ferroelectrics*, vol. 267, no. 1, pp. 403–408, 2002.
- [18] A. Navid, D. Vanderpool, A. Bah, and L. Pilon, "Towards optimization of a pyroelectric energy converter for harvesting waste heat," *Int. J. Heat Mass Transfer*, vol. 53, no. 19–20, pp. 4060–4070, 2010.
- [19] A. Navid, C.S. Lynch, and L. Pilon, "Purified and porous poly(vinylidene fluoride-trifluoroethylene) [P(VDF-TrFE)] thin films for pyroelectric infrared sensing and energy harvesting," *Smart Mater. Struct.*, vol. 19, no. 5, art. no. 055006, 2010.
- [20] G. Sebald, L. Seveyrat, D. Guyomar, L. Lebrun, B. Guiffard, and S. Pruvost, "Electrocaloric and pyroelectric properties of 0.75Pb(Mg_{1/3}Nb_{2/3})O₃-0.25PbTiO₃ single crystals," *J. Appl. Phys.*, vol. 100, no. 12, art. no. 124112, 2006.
- [21] D. Guyomar, S. Pruvost, and G. Sebald, "Energy harvesting based on FE-FE transition in ferroelectric single crystals," *IEEE Trans. Ultrason. Ferroelectr. Freq. Control*, vol. 55, no. 2, pp. 279–285, 2008.
- [22] A. Khodayari, S. Pruvost, G. Sebald, D. Guyomar, and S. Mohammadi, "Nonlinear pyroelectric energy harvesting from relaxor single crystals," *IEEE Trans. Ultrason. Ferroelectr. Freq. Control*, vol. 56, no. 4, pp. 693–699, 2009.
- [23] H. Zhu, S. Pruvost, D. Guyomar, and A. Khodayari, "Thermal energy harvesting from Pb(Zn_{1/3}Nb_{2/3})_{0.955}Ti_{0.045}O₃ single crystals phase transitions," *J. Appl. Phys.*, vol. 106, no. 12, art. no. 124102, 2009.
- [24] R. Kandilian, A. Navid, and L. Pilon, "The pyroelectric energy harvesting capabilities of PMN-PT near the morphotropic phase boundary," *Smart Mater. Struct.*, vol. 20, no. 5, art. no. 055020, 2011.
- [25] I. M. McKinley, R. Kandilian, and L. Pilon, "Waste heat energy harvesting using Olsen cycle on 0.945Pb(Zn_{1/3}Nb_{2/3})O₃-0.055PbTiO₃ single crystals," *Smart Mater. Struct.*, vol. 21, no. 3, art. no. 035015, 2012.
- [26] A. Navid and L. Pilon, "Pyroelectric energy harvesting using Olsen cycles in purified and porous poly(vinylidene fluoride-trifluoroethylene) [P(VDF-TrFE)] thin films," *Smart Mater. Struct.*, vol. 20, no. 2, art. no. 025012, 2011.
- [27] J. Fang, H. Frederich, and L. Pilon, "Harvesting nanoscale thermal radiation using pyroelectric materials," *ASME J. Heat Trans.*, vol. 132, no. 9, art. no. 092701, 2010.
- [28] H. Nguyen, A. Navid, and L. Pilon, "Pyroelectric energy converter using co-polymer P(VDF-TrFE) and Olsen cycle for waste heat energy harvesting," *Appl. Therm. Eng.*, vol. 30, no. 14–15, pp. 2127–2137, 2010.
- [29] A. Cuadras, M. Gasulla, and V. Ferrari, "Thermal energy harvesting through pyroelectricity," *Sens. Actuators A*, vol. 158, no. 1, pp. 132–139, 2010.
- [30] P. Mane, J. Xie, K. Leang, and K. Mossi, "Cyclic energy harvesting from pyroelectric materials," *IEEE Trans. Ultrason. Ferroelectr. Freq. Control*, vol. 58, no. 1, pp. 10–17, 2011.
- [31] S. Hunter, N. Lavrik, T. Bannuru, S. Mostafa, S. Rajic, and P. Datskos, "Development of MEMS based pyroelectric thermal energy harvesters," in *Energy Harvesting and Storage: Materials, Devices, and Applications II*, 2011, art. no. 80350V.
- [32] S. K. T. Ravindran, T. Huesgen, M. Kroener, and P. Woias, "A self-sustaining pyroelectric energy harvester utilizing spatial thermal gradients," in *16th Int. Solid-State Sensors, Actuators and Microsystems Conf.*, 2011, pp. 657–660.
- [33] F. Y. Lee, S. Goljahi, I. McKinley, C. S. Lynch, and L. Pilon, "Pyroelectric waste heat energy harvesting using relaxor ferroelectric 8/65/35 PLZT and the Olsen cycle," *Smart Mater. Struct.*, vol. 21, no. 2, art. no. 025021, 2012.
- [34] F. Y. Lee, A. Navid, and L. Pilon, "Pyroelectric waste heat energy harvesting using heat conduction," *Appl. Therm. Eng.*, vol. 37, pp. 30–37, 2012.
- [35] S. B. Lang and D. K. Das-Gupta, *Handbook of Advanced Electronic and Photonic Materials and Devices*, vol. 4, San Diego, CA: Academic Press, 2001.
- [36] M.W. Hooker, "Properties of PZT-based piezoelectric ceramics between -150 and 250°C," Tech. Rep., Sep. 1998.
- [37] M. E. Lines and A. M. Glass, *Principles and Applications of Ferroelectrics and Related Materials*, Oxford, UK: Clarendon Press, 1977.

- [38] R.B. Olsen, D.A. Bruno, and J.M. Briscoe, "Pyroelectric conversion cycle of vinylidene fluoride-trifluoroethylene copolymer," *J. Appl. Phys.*, vol. 57, no. 11, pp. 5036–5042, 1985.
- [39] S. Kamba, V. Bovton, J. Petzelt, I. Rychetsky, R. Mizars, A. Brilingas, J. Banys, J. Gringas, and M. Kosec, "Dielectric dispersion of the relaxor PLZT ceramics in the frequency range 20 Hz–100 THz," *J. Phys. Condens. Matter*, vol. 12, no. 4, art. no. 497519, 2000.
- [40] G. H. Haertling, "Ferroelectric ceramics: History and technology," *J. Am. Ceram. Soc.*, vol. 82, no. 4, pp. 797–818, 1999.
- [41] D. E. Dausch and G. H. Haertling, "The domain switching and structural characteristics of PLZT bulk ceramics and thin films chemically prepared from the same acetate precursor solutions," *J. Mater. Sci.*, vol. 31, no. 13, pp. 3409–3417, 1996.
- [42] G. H. Haertling and C. E. Land, "Hot-pressed (Pb,La)(Zr,Ti)O₃ ferroelectric ceramics for electro-optic applications," *J. Am. Ceram. Soc.*, vol. 54, no. 1, pp. 1–11, 1971.
- [43] V. Bobnar, Z. Kutnjak, R. Pirc, and A. Levstik, "Electric-field-temperature phase diagram of the relaxor ferroelectric lanthanum-modified lead zirconate titanate," *Phys. Rev. B*, vol. 60, no. 9, pp. 6420–6427, 1999.
- [44] B. Vodopivec, C. Filipic, A. Levstik, J. Holc, and Z. Kutnjak, "E-T phase diagram of the 6.5/65/35 PLZT incipient ferroelectric," *J. Eur. Ceram. Soc.*, vol. 24, no. 6, pp. 1561–1564, 2004.
- [45] D. Viehland, X. H. Dai, J. F. Li, and Z. Xu, "Effects of quenched disorder on La-modified lead zirconate titanate: Long and short-range ordered structurally incommensurate phases, and glassy polar clusters," *J. Appl. Phys.*, vol. 84, no. 1, pp. 458–471, 1998.
- [46] G. Burns and F. H. Dacol, "Crystalline ferroelectrics with glassy polarization behavior," *Phys. Rev. B*, vol. 28, no. 5, pp. 2527–2530, 1983.
- [47] A. A. Bokov and Z. G. Ye, "Recent progress in relaxor ferroelectrics with perovskite structure," *J. Mater. Sci.*, vol. 41, no. 1, pp. 31–52, 2006.
- [48] Z.-G. Ye and H. Schmidt, "Optical, dielectric and polarization studies of the electric field-induced phase transition in Pb(Mg_{1/3}Nb_{2/3})O₃ [PMN]," *Ferroelectrics*, vol. 145, no. 1, pp. 83–108, 1993.
- [49] A. Kholkin, "Piezoresponse force microscopy of polarization dynamics in ferroelectrics," presented at *8th Int. Tutorial Workshop on Piezoresponse Force Microscopy and Nanoscale Electromechanics of Polar Materials*, Beijing, China, August 25–27, 2010.
- [50] M. Akbas, I. Reaney, and W. Lee, "Domain structure-property relations in lead lanthanum zirconate titanate ceramics," *J. Mater. Res.*, vol. 11, no. 9, pp. 2293–2301, 1996.
- [51] D. E. Dausch and G. H. Haertling, "Bulk vs. thin film PLZT ferroelectrics," in *Proc. 8th IEEE Int. Symp. Applications of Ferroelectrics*, 1992, pp. 297–300.
- [52] MG Chemicals, (2012, Jan.) Technical specifications silicon conformal coating (liquid) 422-1L/4L/20L liquid. [Online]. Available: <http://www.mgchemicals.com/downloads/pdf/specsheets/422l.pdf>
- [53] G.H. Haertling, E. Furman, C.S. Hsi, and G. Li, "Superconductivity devices: Commercial use of space," Tech. Rep., Sep. 1993.
- [54] C. Filipic, B. Vodopivec, J. Holc, A. Levstik, Z. Kutnjak, and H. Beige, "Relaxor and incipient ferroelectric phases in 6.5/65/35 PLZT ceramics," *J. Eur. Ceram. Soc.*, vol. 24, no. 6, pp. 1565–1568, 2004.
- [55] J. Yu and M. Ikura, "Direct conversion of low-grade heat to electricity using pyroelectric conversion," in *Proc. Fourth IASTED Int. Conf. Eur. Power and Energy Systems*, 2004, pp. 442–446.
- [56] G. A. Samara, *Ferroelectricity Revisited—Advances in Materials and Physics*. (vol. 56 of *Solid State Physics*), San Diego, CA: Academic Press, 2001, pp. 239–458.
- [57] G. P. Carman, D. Wang, and Y. Fotinich, "Influence of temperature on the electromechanical and fatigue behavior of piezoelectric ceramics," *J. Appl. Phys.*, vol. 83, no. 10, pp. 5342–5350, 1998.
- [58] C. S. Lynch, "Fracture of ferroelectric and relaxor electro-ceramics: Influence of electric field," *Acta Mater.*, vol. 46, no. 2, pp. 599–608, 1998.
- [59] E. Furman and L. E. Cross, "Dielectric breakdown in PLZT 9.5/65/35 ceramics," in *Proc. Ninth IEEE Int. Symp. Ferroelectrics*, 1994, pp. 577–580.
- [60] Y. S. Touloukian, *Thermophysical Properties of Matter*. New York, NY: IFI/Plenum, 1975.
- [61] C. S. Lynch, W. Yang, L. Collier, Z. Suo, and R. M. McMeeking, "Electric field induced cracking in ferroelectric ceramics," *Ferroelectrics*, no. 1, vol. 166, pp. 11–30, 1995.

- [62] J. Nuffer, D. C. Lupascu, and J. Rodel, "Microcrack clouds in fatigued electrostrictive 9.5/65/35 PLZT," *J. Eur. Ceram. Soc.*, vol. 21, no. 1, pp. 1421–1423, 2001.
- [63] B. Fang, Q. Du, L. Zhou, X. Zhao, H. Xu, and H. Luo, "Structural phase transition and physical properties of tetragonal 0.85Pb(Zn_{1/3}Nb_{2/3})O₃-0.15PbTiO₃ single crystals," *J. Appl. Phys.*, vol. 106, no. 7, art. no. 074110, 2009.



Thomas Chin was born in Boston, MA, in 1987. He earned a B.S. degree in mechanical engineering from the University of California, San Diego in 2009 and an M.S. degree in mechanical engineering from the University of California, Los Angeles in 2012.



Felix Lee was born in Hong Kong in 1988 and immigrated to the United States in 1991. He received his B.S. and M.S. degrees in mechanical and aerospace engineering from UCLA in 2010 and 2012, respectively. Felix is currently an engineer at MEA Forensic in Laguna Hills, CA.



Ian M. McKinley was born in Eugene, OR, in 1987 and was raised in Seattle, WA. He received his B.S. degree in mechanical engineering from Columbia University in New York, NY, and his B.A. degree in physics from Occidental College in Los Angeles, CA, in 2010. He is currently a graduate student at UCLA. He is the recipient of the Clean Green IGERT Fellowship supported by the National Science Foundation.



Sam Goljahi was born in Tehran, Iran, on September 21, 1981. His family relocated to the United States shortly after his birth. In 1999, he joined the United States Navy. After his Navy discharge, he earned a bachelor's degree in aerospace engineering from UCLA in 2010. In 2012, he received a master's degree in mechanical engineering, and is currently pursuing his Ph.D. degree.



C. S. Lynch was born in Stoneham, MA, in 1959. He received his B.S.M.E. degree from Cal State Los Angeles, and his M.S.M.E. and Ph.D. degrees from the University of California, Santa Barbara (UCSB). From 1985–1992, Prof. Lynch held the position of staff research engineer at Dynasen Inc., where he was responsible for the design, fabrication, and fielding of custom instrumentation systems for shock wave measurements. From 1993–1995, he held a postdoctoral position at UCSB, where his work focused on characterizing and modeling the large field behavior of ferroelectric materials (constitutive and fracture behavior). In 1995, he joined the faculty at Georgia

Tech and, in 2007, joined the faculty at UCLA as a Professor. His research has continued to focus on smart materials and structures. Prof. Lynch is a Fellow of ASME, and is a member of the ASME Aerospace Division Executive Committee and the ASME Government Relations Committee. He is also a member of SPIE and ASEE. He has been the recipient of a number of awards, including the joint ASME/AIAA Adaptive Structures Prize.



Laurent Pilon was born in Nantes, France, in 1973. He received his B.S. and M.S. degrees in applied physics in 1997 from the Grenoble Institute of Technology and a Ph.D. degree in mechanical engineering from Purdue University in 2002. He then joined the Mechanical and Aerospace Engineering Department at UCLA, where he is now a Professor. He is the recipient of the 2005 National Science Foundation CAREER Award, the 2008 Bergles–Rohsenow Young Investigator Award in Heat Transfer from ASME, and the 2009 Young

Scientist Award in Radiative Transfer from the Journal of Quantitative Spectroscopy and Radiative Transfer. He was elected a Senior Member of SPIE in 2011.